Microphases and Macrophases in Polymer Blends with a Diblock Copolymer

B. Löwenhaupt, A. Steurer, and G. P. Hellmann*

Deutsches Kunststoff-Institut, Schlossgartenstrasse 6, D-6100 Darmstadt, Germany

Y. Gallot

Institut Charles Sadron, 6 rue Boussingault, F-67083 Strasbourg, France

Received April 12, 1993; Revised Manuscript Received October 25, 1993®

ABSTRACT: Blends A/$\alpha\beta$ and C/$\alpha\beta$ of a polymer A or C and a diblock copolymer $\alpha\beta$ with blocks α and β of equal lengths were analyzed, where A is chemically equal to α while C has attractive interactions with α. Films of the blends were cast, using nonselective solvents. The random phase approximation model predicts a transition from microscale to macroscale fluctuations in the still homogeneous solutions, the transition depending on the chain lengths of A or C, relative to that of $\alpha\beta$, on the interactions, in particular those of C and α, and on the temperature. This transition was observed, where predicted, in cast films of various blends of a diblock copolymer P(MMA-*b*-S) of methyl methacrylate and styrene. The microphase and macrophase morphologies of blends with PMMA as well as PS, SAN, poly(cyclohexyl methacrylate), and tetramethyl polycarbonate were characterized by electron microscopy. Effects that are not predicted by the model are shown to come from secondary segregation processes. Quite a variety of morphologies can be produced.

1. Introduction

Blends of homopolymers and block copolymers yield complex morphologies featuring instable macrophases as well as stable microphases.[1–23] This paper deals with blends A/$\alpha\beta$ and C/$\alpha\beta$ of one homopolymer, A or C, and one block copolymer $\alpha\beta$ with two blocks, α and β, of equal length, where, chemically, A = $\alpha \neq \beta$ and C $\neq \alpha \neq \beta$. The morphologies of these blends are characterized by phase domains, as shown in Figure 1 for blends A/$\alpha\beta$.[13] There are two types of morphology that are potentially interesting for different applications.

(1) Blends A/$\alpha\beta$ with domains as in Figure 1a,b have a morphology (but not necessarily also properties) as is known from *impact-modified* thermoplastics.[24] The number of phases can be argued about in these blends. There are two "macrophases", one each of A (matrix) and $\alpha\beta$ (domains). But the domains of $\alpha\beta$ are subdivided into "microphases", one each of α and β ("macro–micro" morphology). It is useful and justified in terms of local thermodynamics to treat these blends as three-phase systems of three components, α, β, and A. The domain in Figure 1a has internally precisely the lamellar two-phase microstructure of the pure copolymer $\alpha\beta$ itself, while the lamellae in the domain in Figure 1b are swollen by the homopolymer.

(2) Blends A/$\alpha\beta$ with micelles as in Figure 1c have only two phases, a macrophase of the chains A and the blocks α (matrix) and a microphase of the blocks β (micellar domains). The blocks α mix with the chains A, while the blocks β do not. This structure, as such, does not raise much interest. But if the corresponding blend B/$\alpha\beta$ has the same type of morphology, only that β mixes with B while α does not, the ternary blend A/B/$\alpha\beta$ is interesting. With α mixing only with A and β only with B, the copolymer $\alpha\beta$ can cover the interfaces in the macrophase morphology produced by A and B, thereby *compatibilizing* the phases.[25–28]

In the classification proposed by Hashimoto et al.,[21–23] concerning the compatibility of A and α, Figure 1 shows

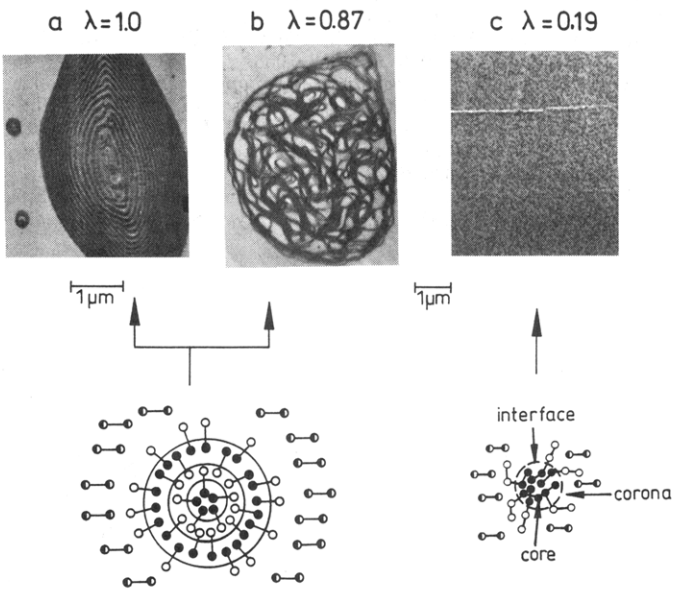

Figure 1. Domains of a diblock copolymer P(MMA-*b*-S) in a matrix of PMMA, the parameter λ describing the chain length ratio of the homopolymer and the copolymer (Table 1): (a), (b) macrophase domains; (c) micelles. Styrene is dark and MMA light.

the cases of "complete segregation" of A and α (Figure 1a), as well as "localized solubilization" (Figure 1b) and "uniform solubilization" (Figure 1c) of α by A.

This paper deals with the question which blends A/$\alpha\beta$ and C/$\alpha\beta$ produce which morphologies. Blends as indicated in Figure 2a were analyzed, by random phase approximation calculations (RPA)[13,15,29–32] and transmission electron microscopy (TEM). In the calculations, the blends C/$\alpha\beta$ will be characterized by two interaction parameters, χ describing bad interactions ($\chi > 0$) between C and β as well as between α and β, and ξ describing good interactions ($\xi < 0$) between C and α. Blends A/$\alpha\beta$ are characterized by $\xi = 0$. The blocks β will always segregate from C (or A) and from α, as they did in Figure 1. The question will be *do C (or A) and α segregate, too,* as they did in Figure 1a,b, or do they mix, as they did in Figure 1c.

* To whom all mail should be sent.

® Abstract published in *Advance ACS Abstracts,* December 15, 1993.

0024-9297/94/2227-0908$04.50/0

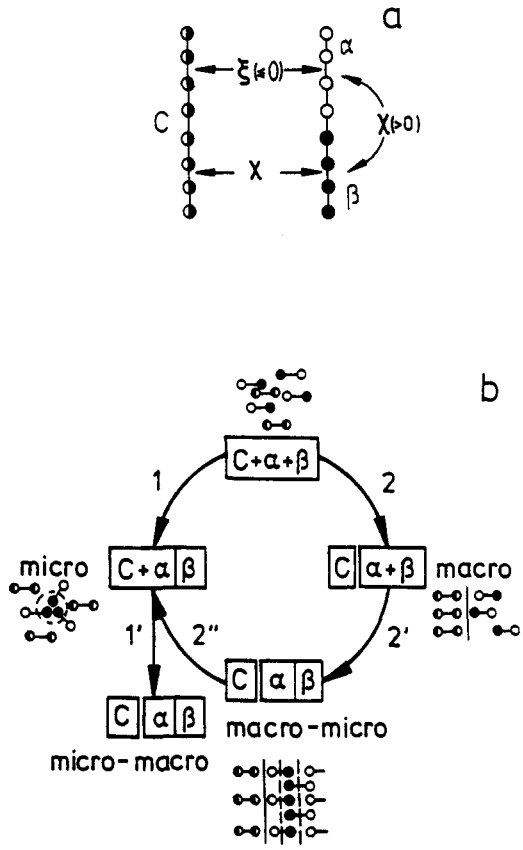

Figure 2. Homopolymer C and diblock copolymer $\alpha\beta$: (a) interaction parameters χ and ξ; (b) phase separation processes in blends C/$\alpha\beta$, "+" indicating miscibility and vertical bars immiscibility.

Most commonly used and discussed are blends A/$\alpha\beta$.[1-23] They are chemically simple and can serve as references for the more complex blends C/$\alpha\beta$. But even the simple constitution of A/$\alpha\beta$ does not guarantee simple morphologies. Microphases and macrophases are observed, depending on the chain lengths ratio of A and $\alpha\beta$, as is witnessed by Figure 1 that shows three blends PMMA/P(MMA-*b*-S) (MMA, methylmethacrylate; S, styrene).

Already the first studies[1,2] on blends A/$\alpha\beta$ revealed that macrophases are formed when the homopolymer A has chains as long as the copolymer $\alpha\beta$ (Figure 1a,b) or longer, which is the normal situation in industries. Macrophases indicate that A and α do not mix with each other, which means that $\alpha\beta$ will not be a good compatibilizer, in ternary blends A/B/$\alpha\beta$. Therefore, it is of interest to assess the chances of avoiding macrophases, i.e. of inducing microphase separation, in blends C/$\alpha\beta$ where A is replaced by a homopolymer C having sufficiently attractive interactions with the block α ($\xi < 0$, Figure 2a). This is discussed below. Briefly, the reversed situation is touched, too, where macrophase separation is induced deliberately.

The process analyzed in this paper is demixing in initially homogeneous systems. Figure 2b shows what can happen. The blend components α, β, and C are at first all in one phase (C + α + β). The main driving force for phase separation is the incompatibility of β both with C and α ($\chi > 0$). It leads either to microphases, when only the blocks α and β segregate from each other (step 1), or to macrophases, when the whole chains C and $\alpha\beta$ segregate from each other (step 2). Figure 1c shows a result of step 1. The macroseparation step 2 is usually followed by a microseparation step 2′ wherein α and β demix, inside the copolymer phase $\alpha\beta$. Results of this "macro-micro" sequence 2 + 2′ are seen in Figure 1a,b.

Other secondary steps of segregation can occur, besides step 2′, which are less easy to understand. There is firstly step 1′ which describes an aggregation of microphases ("micro-macro" sequence 1 + 1′), and secondly step 2″ which describes redissolution of macrophases.

So far, the complexity of Figure 2b has not attracted the attention it deserves. Below, all steps and stages of the figure will be documented, together with transition stages. The main variables will be the chain lengths, the temperature, and the interaction parameter ξ, which control the competition between step 1 and step 2, i.e., between microphases and macrophases.

The homogeneous state (C + α + β, Figure 2b), at which all experiments started, was always established by dissolving the blends in a nonselective solvent. Phase separation was then induced by solvent evaporation, in the process of film casting. Model calculations on the fluctuations in the solutions were carried out to predict the blend morphologies which were analyzed electron microscopically.

2. RPA Calculations

Homogeneous blends C/$\alpha\beta$ of a homopolymer C and a diblock copolymer $\alpha\beta$ having blocks of equal length exhibit a structure of concentration fluctuations that depends mainly (1) on the volume fraction f, the volume per chain $V_{\alpha\beta}$ of the copolymer $\alpha\beta$, and the volume per chain of the homopolymer C, given by the chain length ratio

$$\lambda = v_C/v_{\alpha\beta} \tag{1}$$

and (2) on the interaction parameters χ_{ij} of the pairs C-β, α-β, and C-α. In Figure 2a, repulsive interactions of equal strength are assumed for the pairs C-β and α-β ($\chi_{CB} = \chi_{AB} = \chi > 0$), and attractive interactions for the pair C-α ($\chi_{C\alpha} = \xi \leq 0$).

Phase separation can be studied with these blends C/$\alpha\beta$ if χ is initially small but can be increased considerably, by increasing or decreasing the temperature. Yet, changes of χ are difficult to predict, and appropriate blends are, accordingly, difficult to find. It is easier to study the phase separation of solutions of blends C/$\alpha\beta$ where χ is high. Homogeneity is brought about by dissolving the blends in a nonselective solvent S, and phase separation is induced by concentrating the solutions C/$\alpha\beta$/S again, by removing the solvent. New parameters of the solutions C/$\alpha\beta$/S are (1) the volume fraction ϕ and the molecular volume V_S of the solvent and (2) the interaction parameters involving the solvent, of which there is only one, χ_S, when the solvent is nonselective ($\chi_{CS} = \chi_{\alpha S} = \chi_{\beta S} = \chi_S$). Such solvents were used. They behave merely as neutral diluents for the blends.

Whenever a homogeneous blend approaches the point of phase separation (with or without a solvent), it assumes a pronounced structure of "dominant" fluctuations described by the structure factors

$$\sigma_{ij}(q) = \frac{|\mathbf{M}|_{ij}}{|\mathbf{M}|}(q) \qquad \mathbf{M}_{ij}(q) = \left(\frac{\partial^2 \Delta F}{\partial \phi_i \partial \phi_j}\right)(q) \tag{2}$$

which are obtained by inverting the matrix $\mathbf{M}(q)$ of osmotic compressibilities, on all wave vector scales q. The components i and j of solutions C/$\alpha\beta$/S are C, α, β, and S. The structure factors σ_{ij} depend in the random phase approximation (RPA)[29-32] on the form factors of all components, which characterize the concentration as well as the size and the shape of the different molecules, and on the interaction parameters between the components, as is outlined in detail in ref 13 and, briefly, also in the Appendix.

The parameters used in the following calculations are typical for blends C/$\alpha\beta$ of simple vinyl polymers as, e.g., the blends of PMMA or SAN with the block copolymer P(MMA-*b*-S) considered below. Less important param-

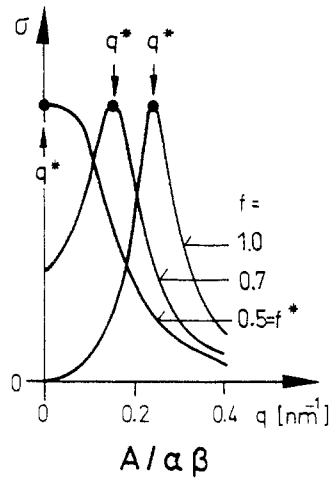

Figure 3. Structure factor σ of solutions ($\phi = \phi^* + 0.05$) of blends A/$\alpha\beta$ differing in the copolymer content f. q^*: characteristic wave vector.

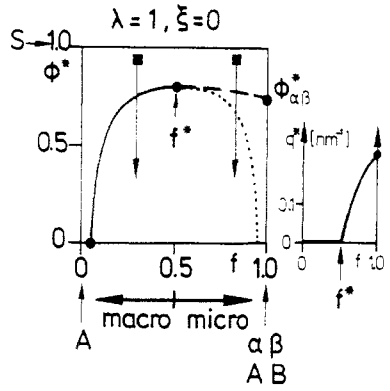

Figure 4. Spinodal solvent concentration ϕ^* of solutions A/$\alpha\beta$/S (—,- -) and A/AB/S (–,··) of different copolymer contents f. f*: transition concentration. Arrows indicate film casting. Small diagram: characteristic wave vector q^* for A/$\alpha\beta$.

eters are specified in the Appendix. Important parameters are (i) $V_{\alpha\beta} = 200$ nm^3, meaning that the copolymer $\alpha\beta$ has a molecular weight in the range (100–150) × 10^3, and (2) $\lambda = 1$ or $\lambda = {}^1/_5$ or $\lambda = 5$, meaning that the homopolymer C has chains as long as the copolymer $\alpha\beta$ or much shorter or much longer, as well as the interaction parameters (Figure 2a) (1) $\chi = 0.2$ nm^{-2}, meaning that β is strongly rejected by C and α, and (2) $\xi < 0$, meaning that C and α are attracted by each other (briefly, $\xi > 0$ is also considered). $V_{\alpha\beta}$ and χ are kept constant while λ and ξ are varied.

Most instructive is the structure factor σ_{ij} of the most rejected component, i.e. the block β. Therefore, the structure factor calculated is

$$\sigma = \sigma_{\beta\beta} = \sigma_{CC} + \sigma_{\alpha\alpha} + 2\sigma_{C\alpha} \qquad (3)$$

The dominant fluctuations in the solutions C/$\alpha\beta$/S are those at the maximum of σ which is positioned at the "characteristic wave vector q^*". These fluctuations are very strong near *the spinodal solvent concentration* ϕ^* which the solutions pass through when the solvent is evaporated off. The parameters q^* and ϕ^* are extracted from the spinodal conditions

$$\sigma(q,\phi) \to \infty \qquad d\sigma(q,\phi/dq) = 0 \qquad (4)$$

2.1. Microphases and Macrophases in Blends A/$\alpha\beta$. RPA results, related to solutions of a blend A/$\alpha\beta$ with $\lambda = 1$, are shown in Figures 3 and 4. The structure factors σ in Figure 3 reveal that blends of different copolymer contents f produce in homogeneous solution very different fluctuation structures. At $f > f^* = 0.5$, σ has a peak at $q^* > 0$, which indicates dominating microscale fluctuations, while, at $f = f^*$ and $f < f^*$, σ decays from a maximum at $q^* = 0$, which indicates dominating macroscale fluctuations. The characteristic wave vector $q^*(f)$ is shown in Figure 4 (small diagram). Clearly, the transition concentration f^* divides the composition scale f of the blends A/$\alpha\beta$ into a range $f < f^*$ and a range $f > f^*$, where macrophases and microphases, respectively, are preformed by the dominant fluctuations in the homogeneous solutions.

The phase diagram predicted for the blend solutions A/$\alpha\beta$/S ($\lambda = 1$) is shown in Figure 4. The miscibility gap (more precisely, the spinodal solvent concentration ϕ^*), is drawn at $f < f^*$ and dashed at $f > f^*$. The copolymer $\alpha\beta$ itself demixes at $\phi_{\alpha\beta}^*$. Two arrows indicate solvent evaporation. As a solution passes through the curve ϕ^*, it demixes, and the fluctuation structure turns into a permanent phase structure. The two-phase morphology that is generated should still be controlled, at first, by the dominant fluctuations. Therefore, the characteristic wave vector q^* should characterize the newly born phase structure, too, which should be of the micro type ($q^* > 0$) at $f > f^*$ (step 1, Figure 2b) and of the macro type ($q^* = 0$) at $f < f^*$ (step 2, Figure 2b).

It is instructive to compare the solutions A/$\alpha\beta$/S with solutions A/AB/S where AB is the random copolymer corresponding to the block copolymer $\alpha\beta$. The two solutions have identical structure factors $\sigma(q = 0)$ and behave thus equally, as far as macrophase separation is concerned. In Figure 4, the spinodal concentration ϕ^* of the solutions A/AB/S is given by the drawn curve at $f < f^*$ and by the dotted curve at $f > f^*$. The solvent evaporation arrow on the right in Figure 4 crosses first the dashed curve ϕ^*, where A/$\alpha\beta$/S undergoes microphase separation, and later the dotted curve, where A/AB/S undergoes (and A/$\alpha\beta$/S would have undergone) macrophase separation. This illustrates that step 1 of Figure 2b occurs, at $f > f^*$, earlier than step 2. At $f < f^*$, on the contrary, it does not matter if $\alpha\beta$ or AB is involved in the blend. When the left hand arrow in Figure 4 passes ϕ^*, both blends undergo macrophase separation.

The model can predict only the primary demixing process, i.e. the process taking pace at ϕ^*. However, there can be secondary segregation processes which can change the morphology, as further solvent is evaporated. Nevertheless, the basic assumption tested in ref 13 and in this paper is that *even the dry blends C/$\alpha\beta$ will usually exhibit those phase structures that were preformed in the homogeneous solutions, i.e. macrophases at $f < f^*$ and microphases at $f > f^*$*. This makes the transition concentration f^* the pivotal parameter. In Figure 4, f^* is in the center, but it moves upward if A is longer-chained ($\lambda > 1$) and downward if A is shorter-chained ($\lambda < 1$), as is shown in Figure 5. The phase diagram for $\lambda = {}^1/_5$ in Figure 6a predicts almost exclusively microphases (step 1, Figure 2b) while Figure 6b for $\lambda = 5$ predicts almost exclusively macrophases (step 2, Figure 2b).

2.2. Induced Microphase Separation. The combination of long homopolymer chains and considerably shorter copolymer chains ($\lambda \gg 1$) is common, particularly in industries. It is of interest to find out if the macrophases of the blend A/$\alpha\beta$ ($\lambda = 5$) (Figure 6b) turn into microphases in blends C/$\alpha\beta$ ($\lambda = 5$), when C and α interact favorably, meaning $\xi < 0$. Macrophases indicate that A or C and α do not mix. Given sufficiently strong attractions of C and α, the two will mix, of course, even at high λ, and microphases will be formed.

Therefore, the question is not can macrophases be turned into microphases at all, but rather, how strong must the C–α attractions be, at least, to lead to the microphases. In

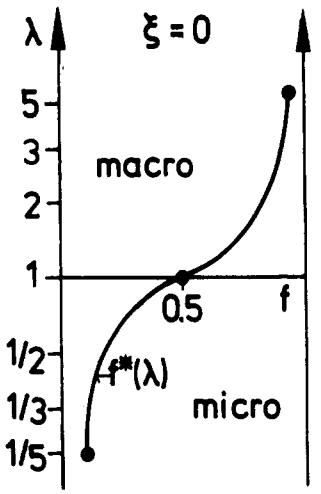

Figure 5. Transition concentration $f^*(\lambda)$ in blends A/$\alpha\beta$ of different chain volume ratios λ (log scale), and predicted regions of macrophase and microphase morphologies.

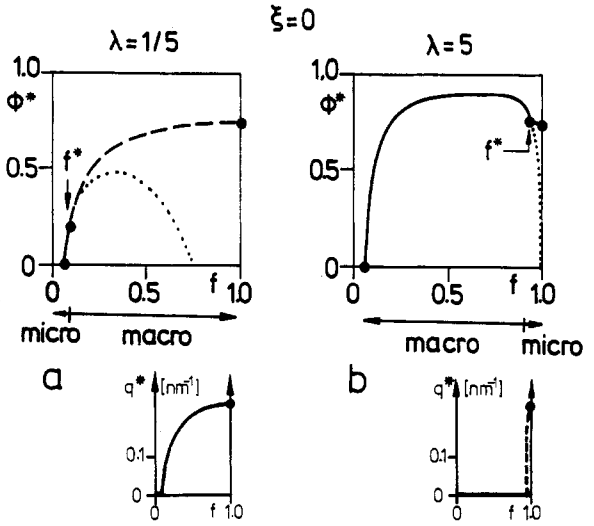

Figure 6. Spinodal solvent concentration ϕ^* of solutions A/$\alpha\beta$/S with (a) $\lambda = 0.2$, (b) $\lambda = 5$ (as in Figure 4).

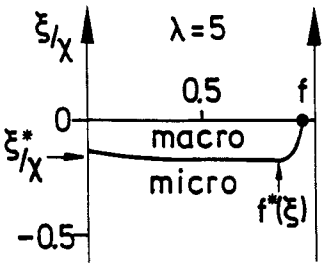

Figure 7. Transition concentration $f^*(\xi)$ in blends C/$\alpha\beta$ ($\lambda = 5$) with different relative interaction parameters ξ/χ, and predicted regions of macrophase and microphase morphologies. The curve f^* ends at the limit ξ^*, below which only microphases are expected.

other words, the question is how restrictive is the condition $\xi < 0$. The answer of the RPA model in Figure 7 is a surprise. The high transition concentration f^* of the blend A/$\alpha\beta$ ($\lambda = 5$, $\xi = 0$) does not change much at first when ξ is decreased into the negative range, in blends C/$\alpha\beta$ ($\lambda = 5$). But then a sudden drop $f^* \to 0$ is predicted, at a moderately negative ξ^*. Below ξ^*, microphase separation should prevail, exclusively.

A comparison of Figures 6b and 8 reveals details. Decreasing ξ reduces the macrophase miscibility gap (dotted) much faster than the microphase miscibility gap (dashed). In Figure 8b, where $\xi < \xi^*$, the two gaps are out of contact, microphases being formed, at all f, earlier than macrophases.

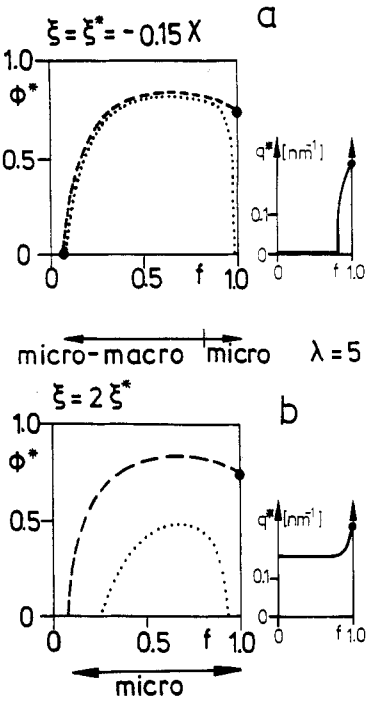

Figure 8. Spinodal solvent concentration ϕ^* of solutions C/$\alpha\beta$/S and C/AB/S ($\lambda = 5$) with different interaction parameters: (a) $\xi = \xi^*$; (b) $\xi = 2\xi^*$ (as in Figure 4).

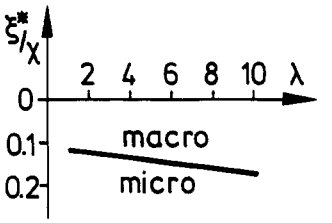

Figure 9. Limiting interaction parameter ξ^* of blends C/$\alpha\beta$ as a function of the chain volume ratio λ. Below ξ^*, only microphases are expected.

In conclusion, lowering ξ, at $\lambda = 5$ (Figures 6b and 8a,b), has the same consequences as lowering λ, at $\xi = 0$ (Figures 6b, 4, and 6a). Figure 9 shows the critical ratio of interaction parameters ξ^*/χ as a function of the chain length ratio λ. It turns out that, regardless of λ, ξ^* does not have to be very negative, meaning that the attractive interactions between C and α *do not have to be strong* to lead to microphases. This is fortunate, as it raises hopes that blends with $\xi < \xi^*$ will not be too difficult to find, even though even $\xi < 0$ is rare.

2.3. Induced Macrophase Separation. The inverse question is can macrophase separation be induced in blends C/$\alpha\beta$ with $\lambda = 1/5$, where the homopolymer chains are short and the blend A/$\alpha\beta$ yields almost exclusively microphases (Figure 6a). As expected, repulsion between C and α, i.e. $\xi > 0$, shifts the transition concentration f^* upward, as is shown in Figure 10, but the shift is only gradual. These blends are not in any way special. There is no limit ξ^* in Figure 10, as there was in Figure 7. It takes blends with $\xi \simeq \chi$ for predominant macrophase separation. Finding blends with such strong repulsions between all components is trivial.

3. Experimental Section

The polymers are characterized in Table 1. The block copolymer was made via anionic polymerization, the polymers PMMA, PS, SAN (azeotropic copolymer of styrene and acrylonitrile), and PCHMA (poly(cyclohexyl methacrylate)) were made via radical polymerization, and PC and TMPC (the polycarbonates of Bisphenol A and

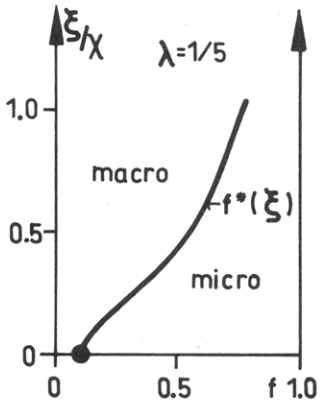

Figure 10. Transition concentrations $f^*(\xi)$ in blends C/$\alpha\beta$ (λ = 0.2) with different relative interaction parameters ξ/χ, and predicted rections of macrophase and microphase morphologies.

Table 1. Polymers

	M_w	$\frac{M_w}{M_n}$	λ
P(MMA-*b*-*S*)	175 000	1.04	
PMMA	35 000	2.0	0.19
	95 000	1.9	0.50
	161 000	2.0	0.87
	188 000	2.2	1.0
	220 000	1.9	1.2[a]
	535 000	2.0	2.9
PS	208 000	2.0	1.3
SAN	215 000	2.2	1.3[a]
PCHMA	212 000	2.4	1.2
PC	31 000	2.3	0.17
TMPC	183 000	2.4	1.1

[a] Used for the blends (SAN/PMMA).

tetramethyl Bisphenol A) were made by Bayer AG via phase transfer polycondensation. The molecular weights were determined by GPC, using PMMA or PS calibration or, for the block copolymer, both averaged, by PC calibration (for PC and TMPC). The block copolymer was also analyzed by LALLS. The parameter $\lambda = V_C/V_{\alpha\beta}$ is the chain volume ratio of eq 1.

Films of the blends were cast at different temperatures as described in ref 33, using toluene for PMMA blends and THF otherwise. TEM pictures were made with an Elmiskop 1a (Siemens AG), using thin sections. Contrast was obtained by selective degradation of the MMA chains and blocks in the electron beam. In the blends with PS, SAN, and TMPC, the contrast was enhanced by staining with RuO_4. PMMA appears white in the electron micrographs.

4. Results

The morphologies of blend films A/$\alpha\beta$ and C/$\alpha\beta$, cast from solution, were investigated and compared to the RPA model predictions. Agreement of observation and theory was taken to prove that the blend morphology had been preformed in solution, while disagreement was believed to indicate that the morphology was altered, after the primary demixing step, by secondary segregation steps.

The following analysis is focused on the transition from microphase to macrophase structures occurring when the chain volume ratio λ, the interaction parameter ξ, or the temperature is varied. Some issues of ref 13 will be picked up again.

4.1. Chain Volume Ratio (Blends A/$\alpha\beta$). The types of morphology found in films of blends PMMA/P(MMA-*b*-S) differing in chain volume ratio λ are indicated in Figure 11, together with the RPA prediction $f^*(\lambda)$.[13] The model agrees fairly well with the data.

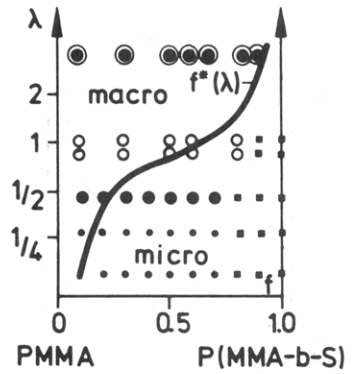

Figure 11. Transition concentrations $f^*(\lambda)$ (calculated) of blends PMMA/P(MMA-*b*-S) differing in λ, and phase morphologies (observed): (·) micelles; (■) lamellae; (●) micelle aggregates; ○, ⊙: macrophases (stable only at low (○) or at all (⊙) temperatures).

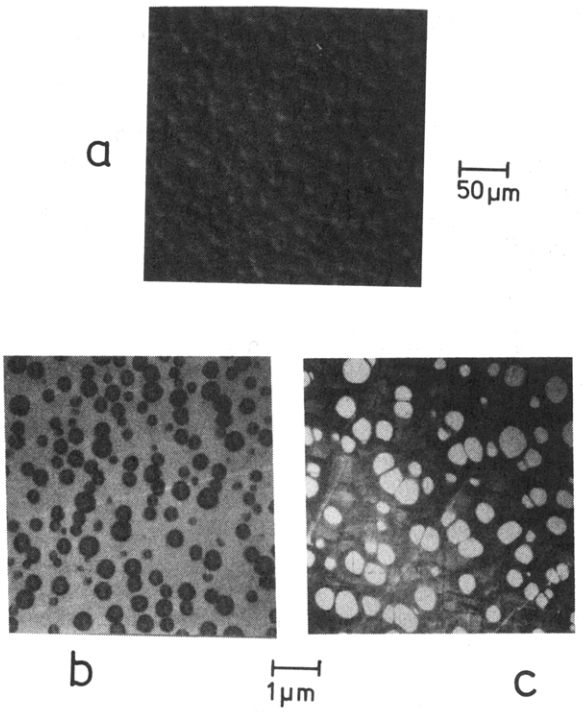

Figure 12. Blend PMMA/P(MMA-*b*-S) (λ = 2.9) with f = 0.30, at 60 °C: (a) light micrograph; (b), (c) electron micrographs.

Blends with short-chained PMMA ($\lambda < 0.5$) yielded transparent films with microphase structures (step 1, Figure 2b), in the form of either of micelles as in Figure 1c or, at $f \geq 0.8$, of lamellae as formed by the pure copolymer itself. (This lamellar structure is seen inside the domain in Figure 1a.)

Blends with long-chained PMMA ($\lambda > 1$) yielded opaque films with coarse macrophase morphologies, as shown in the light micrograph of Figure 12a. The investigation of such structures can be grossly misleading, if only electron microscopy is employed, as is illustrated by Figure 12b,c. The impression from Figure 12b is that P(MMA-*b*-S) forms tiny macrophases in a matrix of PMMA, while the roles are reversed in Figure 12c. Yet, both pictures come from the same film, i.e. that of Figure 12a. The very small domains in Figure 12b,c are merely substructures inside much larger macrophases. (The domain in Figure 1d of ref 13 is also such a substructure, which was not recognized at the time.)

This error is dangerous inasmuch as blends with shorter-chained PMMA, in the range $\lambda \simeq 1$, yield practically the same morphologies, as is shown in Figure 13. The patterns are here, however, not substructures of larger domains.

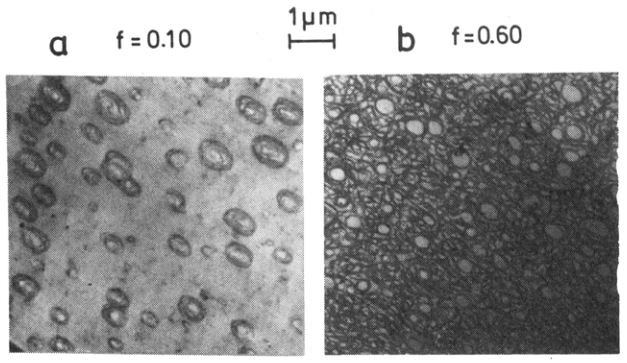

Figure 13. Blends PMMA/P(MMA-*b*-S) (λ = 0.87) with (a) f = 0.10 and (b) f = 0.60 at 60 °C.

PMMA is the matrix at low f and the copolymer at high f.

At intermediate compositions f, the blends with $\lambda \simeq 1$ exhibit cocontinuous phase structures, as shown in Figure 14a for $\lambda = 0.87$. This is an important observation, because cocontinuous phase networks are characteristic of homopolymer blends (Figure 14b). The macrostructures for the blends PMMA/P(MMA-*b*-S) and PMMA/PS in Figure 14 are evidently equal. Figure 14a is, therefore, solid proof that the block copolymer blend has demixed, in the primary process, via macrophase separation (step 2, Figure 2b). The lamellar structure inside the copolymer phase was obviously formed in a secondary process (sequence 2 + 2′ "macro–micro", Figure 2b). (It should be emphasized that the blends with $\lambda > 1$ exhibit cocontinuous phase networks, too. That Figure 12a shows spherical domains instead is only due to a breakup of networks that occurs when the structures become coarser than the film thickness. This effect is discussed in ref 33.)

The transition from micro to macro structures was found in the blends PMMA/P(MMA-*b*-S) with $\lambda = 0.50$. When films were cast rapidly, these blends yielded exclusively micelles, indicating that microphases are produced in the primary demixing process. But slower casting yielded micelles together with larger domains, as shown in Figure 15. The domains look like spherulites and exhibit internally a lamellar microstructure.

Peculiar about these blends is that a high copolymer content f does not provoke a matrix inversion. The domains grow always in the matrix of the homopolymer, as do crystalline spherulites, even if the copolymer is the major component (Figure 15b). That the copolymer refuses to take over the matrix role at high f is entirely atypical for macrophase structures and much in contrast to the behavior of blends with $\lambda \cong 1$ (Figure 13b). The domains in Figure 15 must result from aggregation of the micelles in a secondary process (sequence 1 + 1′ "micro–macro", Figure 2b).

In summary, micelles (step 1) are formed, when $\lambda < 0.50$, macrophases (sequence 2 + 2′), when $\lambda > 0.50$, and micelle aggregates (sequence 1 + 1′, Figure 2b), at $\lambda = 0.50$. In this transition range, microphases are preformed in the homogeneous solutions and lead primarily to micelles, but the aggregates are, in fact, thermodynamically favored. The pictures characterizing the different morphologies best are Figure 1c for micelles, Figure 15a for aggregates, and Figure 14a for macrophase networks.

4.2. Interactions (Blends C/$\alpha\beta$). According to Figure 9, all blends C/$\alpha\beta$, even those with $\lambda > 1$, should feature microphases when C and α attract each other sufficiently, i.e. when $\xi < \xi^*$. This was likely to be the case in a series of blends where C was one of the polymers PCHMA, TMPC, and SAN, and $\alpha\beta$ was the block copolymer P(MMA-*b*-S). The blends PS/PCHMA,[34] PS/TMPC,[35] and PMMA/SAN[36] are always homogeneous, regardless of chain lengths, meaning that the chains C interact in the above blends C/$\alpha\beta$ always favorably with one of the blocks, α or β ($\xi < 0$, Figure 2a). (To fit into the scheme for blends C/$\alpha\beta$ in Figure 2a, the copolymer must be written in the form "P(MMA-*b*-S)" for blends with SAN, but "P(S-*b*-MMA)" for blends with PCHMA or TMPC.) Blends with the constant copolymer content f = 0.4 were analyzed. The chain volume ratios are $1.1 < \lambda < 1.3$ (Table 1), which is high enough to yield opaque films with macrophase morphologies in the blends A/$\alpha\beta$ with PMMA (Figure 16a, v = 0) and the blends B/$\alpha\beta$ with PS (Figure 16b). In contrast, all the blends C/$\alpha\beta$ yielded transparent films with micellar structures.

The micelles are shown in Figure 16a (v = 1) for the blend SAN/P(MMA-*b*-S). To study the transition from micro to macro structures, ternary blends (SAN + PMMA)$_v$/P(MMA-*b*-S)$_{f=0.4}$ were prepared, where the homogeneous blend (SAN + PMMA)$_v$ (v: volume fraction of SAN) plays the role of "polymer C". A decrease from v = 1 to v = 0 amounts to an increase of the interaction parameter ξ from $\xi < \xi^*$ to ξ = 0. As is shown in the turbidity diagram of Figure 17, the films of the ternary blends were opaque below and transparent above v = 0.6, which is evidently the transition stage where $\xi = \xi^*$.

Morphologies of the blends ((SAN + PMMA)$_v$/P(MMA-*b*-S)$_{f=0.4}$ are shown in Figure 16a. The transition from

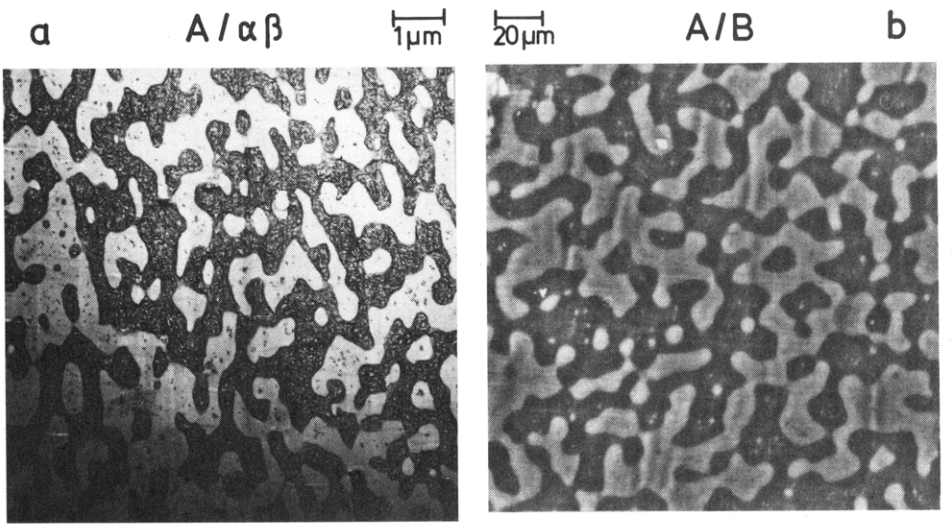

Figure 14. Cocontinuous structures in blends (a) PMMA/P(MMA-*b*-S) (λ = 0.87) with f = 0.30 and (b) PMMA/PS with f = 0.50 at 60 °C.

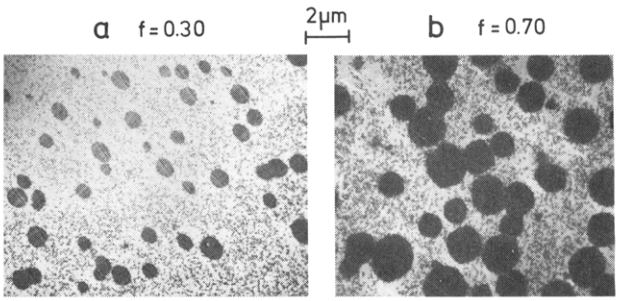

Figure 15. Micelles and micelle aggregates in blends PMMA/P(MMA-*b*-S) ($\lambda = 0.50$) with (a) $f = 0.30$ and (b) $f = 0.70$ at room temperature.

micelles to macrostructures is not of the type of micelle aggregates as in Figure 15. The spherical micelles turn, in Figure 16a, at $v = 0.7$ into lamellae that are separated by matrix polymer. This transition stage is easily explained: Spherical micelles provide a maximum of contact between chains C and blocks α. As C and α interact less favorably, this surface should be reduced by a transition from spheres to lamellae. Still less attractive interactions should make the lamellae aggregate. The lamellae at $v = 0.7$ in Figure 16a are already partly aggregated, indicating that the structure is exactly on the borderline of micro and macro morphologies.

This structure of swollen, aggregated lamellae seems a very logical transition stage. Yet, the spherical micelles aggregated in Figure 15 directly, without the lamellar transition stage. Why is not entirely clear yet.

In summary, the model prediction of Figure 9 that the C–α attractions do not have to be strong to remove all macrophases from the blends C/$\alpha\beta$ seems to be valid. All of the above polymers C that form homogeneous blends C/A or C/B, indicating $\xi < 0$, yielded micellar structures in the blends C/$\alpha\beta$, meaning that even $\xi < \xi^*$. This suggests that ξ^* is not very negative. Interesting transition structures, as that in Figure 16a ($v = 0.7$), can always be designed using blends (A + C)/$\alpha\beta$. Alternatively, blends A-*co*-C/$\alpha\beta$ with a random copolymer A-*co*-C of A and C could be used.

So far, the important situation ($\lambda > 1$, $\xi < 0$) was considered. In comparison, the reversed situation ($\lambda < 1$, $\xi > 0$) is not attractive. Blends with $\xi > 0$ are all too common, and $\lambda < 1$ is usually avoided because short-chained polymers are brittle. Various blends C/$\alpha\beta$ of this type were tested. Figure 10 predicts mostly microphases, yet macrophases were found in all cases at most compositions, even in the blend PC/P(MMA-*b*-S) ($\lambda = 0.17$), although the homopolymer blend PMMA/PC is close to miscibility,[37] meaning that $\xi > 0$ is small. The RPA model seems to be less suited for blends where all interactions are bad ($\xi > 0$).

4.3. Temperature (Blends A/$\alpha\beta$). Of all parameters that control the structure factor σ of the blends A/$\alpha\beta$, only the interaction parameter χ is sensitive to temperature (since $\xi = 0$). According to the RPA model, χ is unimportant for the transition concentration f^*. Therefore, the distribution of micro and macro structures should not depend on temperature.

Nevertheless, blends PMMA/P(MMA-*b*-S) with $0.5 \leq \lambda \leq 1$ undergo a transition from macro to micro structures at elevated temperatures. The phase diagram in Figure 18 for $\lambda = 0.87$ features a macrophase miscibility gap below the critical temperature $T_c \cong 100$ °C. The diagram was measured by casting films at the temperatures and compositions indicated by the symbols. The different types of morphology are shown in the indicated figures.

Only one structure is new. It is shown in Figure 19. In

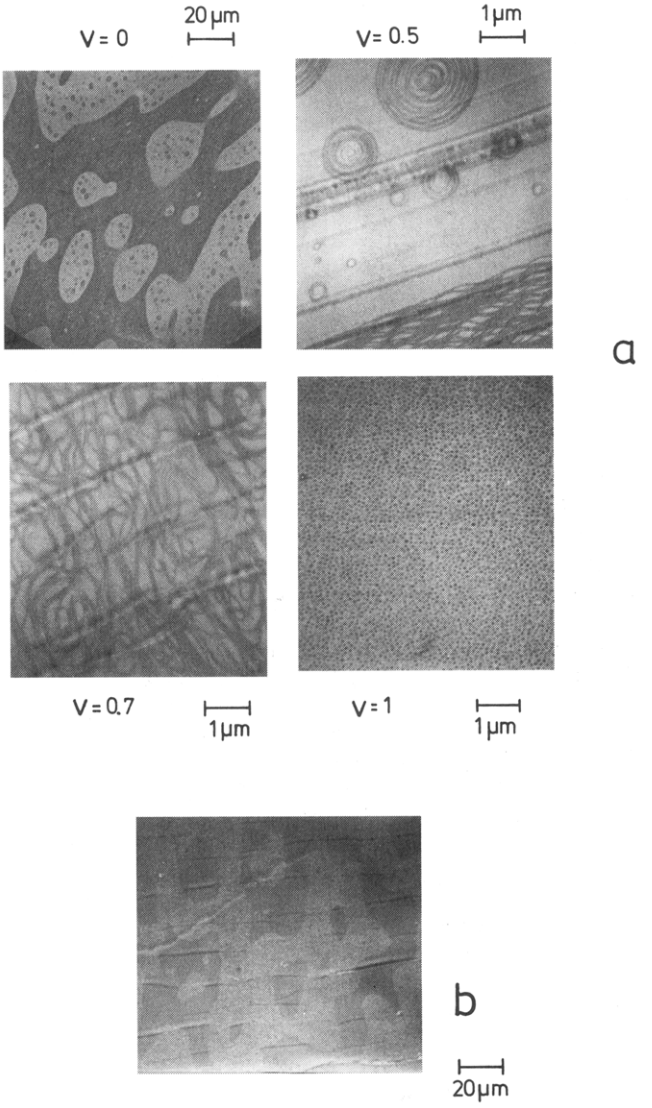

Figure 16. Blends (a) ((SAN+PMMA)$_v$/P(MMA-*b*-S)$_{f=0.40}$ (v, volume fraction of SAN in the binary blend; f, volume fraction of the copolymer in the ternary blend) and (b) PS/P(MMA-*b*-S)$_{f=0.40}$ at room temperature.

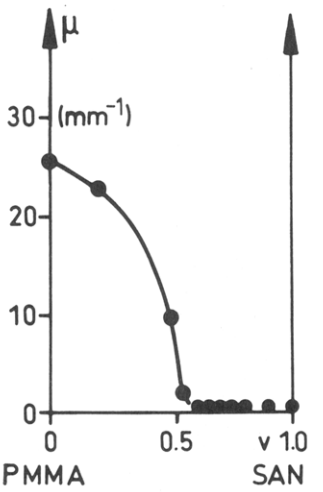

Figure 17. Turbidity of blend films (SAN/PMMA)$_v$/P(MMA-*b*-S)$_{f=0.40}$ in white light, in terms of the attenuation coefficient μ of Lambert's law $(I/I_o) = e^{-\mu d}$, where I and I_o are the transmitted and original light intensity and d is the film thickness.

the range just above T_c, lamellar structures are observed in a broad range of compositions. At lower f, the lamellae are not as perfect as in Figure 16a ($v = 0.7$). They are rather ribbons and cylinders.

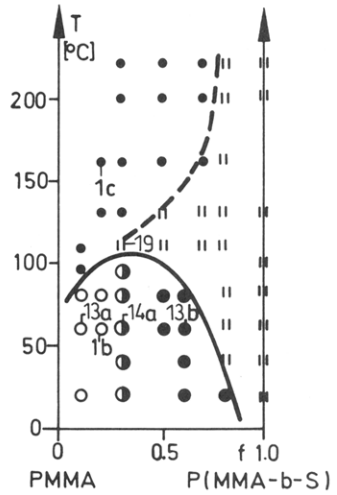

Figure 18. Phase diagram of the blend PMMA/P(PMMA-*b*-S) ($\lambda = 0.87$): (·) micelles; (‖) lamellae; (○, ◑, ●) macrophases (○, matrix PMMA; ◑, cocontinuous; ●, matrix P(MMA-*b*-S)). The numbers indicate the figures with electron micrographs.

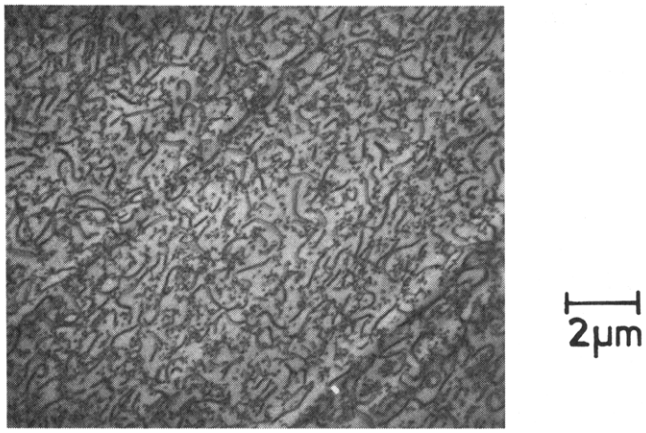

Figure 19. Blend PMMA/P(MMA-*b*-S) ($\lambda = 0.87$) with $f = 0.30$ at 110 °C.

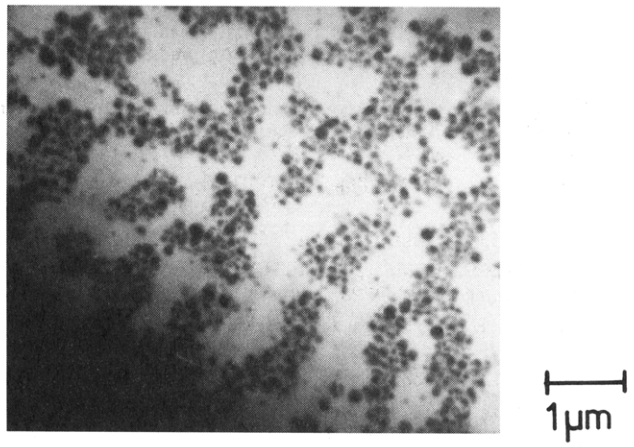

Figure 20. Blend PMMA/P(MMA-*b*-S) ($\lambda = 0.87$) with $f = 0.30$ first cast at 60 °C (Figure 14a) and then annealed 4 h at 200 °C.

To rule out the possibility that the microphases at high temperatures are due to too fast film casting, dry blend films with a macrophase morphology were heated to high temperatures. The macrostructures disintegrated, leaving in the end only randomly dispersed micelles. Figure 20 shows an early stage of this process. The initial cocontinuous morphology (Figure 14a) is still preserved, but the lamellar substructure has already given way to spherical micelles.

Clearly, the macrophases are destabilized at elevated temperatures, and the question is why. The RPA model was so far successful enough to deserve credit. It predicts macrophases for all temperatures in Figure 18 (at $f \leq 0.5$, Figure 4). Assuming that these had indeed always been formed in the primary segregation process (step 2, Figure 2b), even at high temperatures, the microphases observed at $T > T_c$ must come from a redissolution of the macrophases, i.e. from the sequence $2 + 2' + 2''$ in Figure 2b. This sequence is not at all extraordinary.

The primary macrophase separation step 2 occurs due to the incompatibility of the chains A and the blocks β. But, as soon as α and β have subsequently demixed into microphases, in the secondary step 2′, A and β are out of contact, being separated by the blocks α. Thereby, the reason for the initial step 2 is eliminated, and the macrophases should redissolve, in step 2″.

This suggests even that microphases, formed via step 1 or the sequence $2 + 2' + 2''$, are the only thermodynamically stable morphology in blends A/$\alpha\beta$. Macrophases would owe their existence only to kinetic hindrance of the redissolution step 2″. Yet, this is disproved by Figure 15, where the micelles aggregate voluntarily, forming macrophases via the sequence $1 + 1'$. Slow kinetics may hinder step 2″, but they certainly cannot promote step 1′. Another proof for the stability of macrophases is that they appear in blends with $\lambda > 1$ at all temperatures, even far above the glass transition (100–120 °C) where kinetic effects do not interfere. The critical temperature, which is $T_c \cong 100$ °C ($\lambda = 0.87$) in Figure 18, is a monotonously increasing function of the chain length ratio λ.[13] The micelle aggregates in Figure 15 are also dissolved at elevated temperature, the critical temperature being $T_c \cong 30$ °C ($\lambda = 0.50$).

The conclusion is that the macrophases, formed via the sequences $1 + 1'$ or $2 + 2'$, are indeed stable at low temperatures. The phase diagram in Figure 18 should not be far from equilibrium. The remaining problem is to understand why the macrophases are in blends with $0.5 < \lambda < 1$ stable at low, but not at high temperatures. This is discussed most conveniently in terms of the aggregation and deaggregation of micelles.

There are two explanations. A micelle, with β in the core and α in the corona, surrounded by A (Figure 1c) is considered.

(1) Entropy Loss. Blocks α and chains A cannot mix properly in the corona while Gaussian coil conformations are simultaneously assumed. To achieve an even density, both must deform their coils, whereby they lose entropy. Model calculations by Xie et al.,[17] based on Helfand's model[38] on the microstructures of block copolymers, indicate that this entropy loss can cause A and α to segregate, which leads to micelle aggregation.

(2) Incomplete Screening. Blocks α in the corona screen the blocks β in the core from the chains A. But the screening is perfect, so that A and β are out of contact, only when there are strong repulsions between α and β, i.e. at high χ. Weak repulsions at low χ lead to an ill-defined, broad interface between core and corona and thus to inefficient screening. A and β are still in contact which can induce macrophase separation.

Neither effect invokes repulsions between A and α ($\xi > 0$), which would be hard to understand. Both effects can explain why macrophases can be stable, in blends A/$\alpha\beta$. But the effect of entropy loss, which undoubtedly exists, does not seem to explain the destabilization of macrophases at high temperatures. The effect of incomplete screening seems better suited to explain a macro to micro transition in the direction of increasing temperature, because the interaction parameter χ increases with temperature, as was demonstrated in investigations on blends PMMA/P(MMA-*co*-S) with random copolymers.[39] In terms of this

effect, micelle aggregates and macrophases are stable only as long as χ is small. At high temperatures, they disintegrate into micelles, because the high χ sharpens the interfaces of the micelles. The MMA blocks (α) cover perfectly the styrene blocks (β) which are thus invisible for the homopolymer chains PMMA (A).

5. Conclusion

Morphologies of microphases, macrophases, or transition stages between the two can be prepared in blends A/$\alpha\beta$ and C/$\alpha\beta$ by varying the homopolymer–copolymer chain length ratio, the C–α interactions, or the temperature. The transition structures are of the types of micelle aggregates or of homopolymer-swollen lamellar arrays.

In blends A/$\alpha\beta$, these different morphologies can only be designed by adjusting the molecular weights. That is usually easy but has the drawback that microphases are often obtained only when short-chained homopolymers are used. Blends C/$\alpha\beta$ have the distinct advantage that the interactions of C and α can be adjusted, so that short chains can be avoided. A problem is that attractive C–α interactions are needed, which are not always easy to find. However, it emerges from the above calculations and was supported by the experiments that the attractive forces do not have to be strong. There is hope that suitable C–α pairs exist in many cases. Once an attractive pair C–α is found, all different micro and macro morphologies can be produced using blends (A + C)/$\alpha\beta$ or, as will be demonstrated in a forthcoming paper, also blends A-*co*-C/$\alpha\beta$, where (A + C) is a (automatically homogeneous) binary blend and A-*co*-C is a random copolymer.

Acknowledgment. This AIF project (No. 8472) was financially supported by the Bundesminister für Wirtschaft. We thank J. P. Lingelser from the Institut Charles Sadron for the preparation of the block copolymer.

Appendix

The matrix **M** of eq 2 takes for solutions of the blends C/$\alpha\beta$ specified in Figure 2a the form

$$\mathbf{M} = \{\mathbf{X}\} + \begin{Bmatrix} \frac{1}{S_C} & \xi & \chi \\ \xi & \frac{S_1}{\Delta S} & \chi + \frac{S_1 - S_2/2}{\Delta S} \\ \chi & \chi + \frac{S_1 - S_2/2}{\Delta S} & \frac{S_1}{\Delta S} \end{Bmatrix} \quad \text{(A.1)}$$

where the abbreviations $\Delta S = S_2(S_1 - S_2/4)$ and $\{\mathbf{X}\}$, a matrix with equal elements $X = 1/S_S - 2\chi_S$, were used. The special case of blends A/$\alpha\beta$, where $\xi = 0$, is treated theoretically in ref 13.

The molecular form factors are S_C for the polymer chains C and S_2 for the chains and S_1 for the blocks of the copolymer $\alpha\beta$, as well as S_S for the solvent molecules. These form factors are given by

$$S_i = \phi_i V_i g_i \qquad i = C, 2, 1, S \quad \text{(A.2)}$$

ϕ_i: volume fraction

V_i: volume per chain

$g_i = \frac{2}{x}\left(1 - \frac{1}{x}(1 - e^{-x})\right)$, $x = V_i C_i^2/(6q^2)$: Debye function

C_i: square chain stiffness parameter

The parameters used in this paper are $V_S = 0.2$ nm^3 and $\chi_S = 2$ nm^{-3}, which involve the solvent, and for the polymers, $V_{\alpha\beta} = 200$ nm^3, $V_C = \lambda V_{\alpha\beta}$, and $C^2 = 2$ nm^{-1} (for all polymers, $C_S^2 = 0$).

References and Notes

(1) Riess, G.; Kohler, J.; Tournut, C.; Banderet, A. *Makromol. Chem.* **1967**, *101*, 58.
(2) Riess, G.; Jolivet, Y. *Adv. Chem. Ser.* **1975**, *142*, 243.
(3) Inoue, T.; Soen, T.; Hashimoto, T.; Kawai, H. *Macromolecules* **1970**, *3*, 87. *Block Copolymers*; Aggarwal, S., Ed.; Plenum: New York, 1970; p 53.
(4) Eastmond, G. C.; Phillips, D. G. *Polymer* **1979**, *20*, 1501.
(5) Shibayama, M.; Hashimoto, T.; Hasegawa, H.; Kawai, H. *Macromolecules* **1983**, *16*, 1427.
(6) Zin, W. C.; Roe, R. J. *Macromolecules* **1984**, *17*, 183, 189.
(7) Jiang, M.; Huang, X.; Yu, T. *Polymer* **1983**, *24*, 1259; **1986**, *27*, 1923.
(8) Sardelis, K.; Michels, H. J.; Allen, G. *Polymer* **1987**, *28*, 244.
(9) Kinning, D. J.; Winey, K. I.; Thomas, E. L. *Macromolecules* **1988**, *21*, 3502.
(10) Roe, R. J.; Rigby, D. *Adv. Polym. Sci.* **1987**, *82*, 103.
(11) Aggarwal, S. L. *Polymer* **1976**, *17*, 938.
(12) Jiang, M.; Xie, H. *Prog. Polym. Sci.* **1991**, *16*, 977.
(13) Löwenhaupt, B.; Hellmann, G. P. *Polymer* **1991**, *32*, 1065.
(14) Meier, D. *Polym. Prepr. (Am. Chem. Soc., Div. Polym. Chem.)* **1977**, *18*, 340.
(15) Leibler, L.; Orland, H.; Wheeler, J. C. *J. Chem. Phys.* **1983**, *79*, 3550.
(16) Hong, K. H.; Noolandi, J. *Macromolecules* **1983**, *16*, 1083.
(17) Xie, H.; Liu, Y.; Jiang, M.; Yu, T. *Polymer* **1986**, *27*, 1928.
(18) Tanaka, H.; Hashimoto, T. *Polym. Commun.* **1988**, *29*, 212.
(19) Bates, F.; Berney, C. V.; Cohen, R. E. *Macromolecules* **1983**, *16*, 1101.
(20) Winey, K. I.; Thomas, E. L.; Fetters, L. J. *Macromolecules* **1991**, *24*, 6182.
(21) Tanaka, H.; Hasegawa, H.; Hashimoto, T. *Macromolecules* **1991**, *24*, 240.
(22) Hashimoto, T.; Tanaka, H.; Hasegawa, H. *Macromolecules* **1990**, *23*, 4378.
(23) Tanaka, H.; Hashimoto, T. *Macromolecules* **1991**, *24*, 5713.
(24) Bucknall, C. B. *Toughened Plastics*; Applied Science Publishers: London, 1977.
(25) Paul, D. R. Interfacial Agents ("Compatibilizers") for Polymer Blends. In *Polymer Blends*; Paul, D. R., Newman, S., Eds.; Academic Press: New York, 1978.
(26) Fayt, D.; Jerome, R.; Theyssie, P. *Polym. Eng. Sci.* **1987**, *27*, 328.
(27) Barlow, J. W.; Paul, D. R. *Polym. Eng. Sci.* **1984**, *24*, 525.
(28) Shull, K. R.; Kramer, E. J.; Hadziioannou, G.; Tang, W. *Macromolecules* **1990**, *23*, 4780.
(29) Ornstein, L. S.; Zernicke, T. *Proc. Acad. Sci. Amsterdam* **1914**, *17*, 793.
(30) Leibler, L. *Macromolecules* **1980**, *13*, 1602.
(31) Benoit, H.; Wu, W.; Benmouna, M.; Mozer, B.; Bauer, B.; Lapp, A. *Macromolecules* **1985**, *18*, 986.
(32) Mori, K.; Tanaka, T.; Hashimoto, T. *Macromolecules* **1987**, *20*, 381.
(33) Yu, D.; Andradi, L. N.; Hellmann, G. P. *Makromol. Chem.* **1991**, *192*, 2615.
(34) Siol, W. *Makromol. Chem., Macromol. Symp.* **1991**, *44*, 47.
(35) Casper, R.; Morbitzer, L. *Angew. Makromol. Chem.* **1977**, *58/59*, 1.
(36) Stein, D. J.; Jung, R. H.; Illers, K. H.; Hendus, H. *Angew. Makromol. Chem.* **1974**, *36*, 89.
(37) Butzbach, G. D.; Wendorff, J. H. *Polymer* **1991**, *32*, 1155.
(38) Helfand, E.; Wasserman, Z. *Macromolecules* **1976**, *9*, 879; **1978**, *11*, 960; **1980**, *13*, 994.
(39) Kohl, P. R.; Seifert, A. M.; Hellmann, G. P. *J. Polym. Sci., Polym. Phys. Ed.* **1990**, *28*, 1309.